

## DIRECT NUMERICAL SIMULATIONS OF HYDROGEN-ENRICHED METHANE/AIR TURBULENT SWIRLING PREMIXED FLAMES

Joonhwi Park, Yuki Minamoto, Masayasu Shimura, Mamoru Tanahashi

Department of Mechanical Engineering  
Tokyo Institute of Technology  
2-12-1 Ookayama, Meguro-ku, Tokyo 152-8550, Japan  
park.j.ae@m.titech.ac.jp

### ABSTRACT

Direct numerical simulations of H<sub>2</sub>-enriched CH<sub>4</sub>/air turbulent swirling premixed flames in a cuboid combustor have been performed to clarify effects of hydrogen enrichment on the flame structures in a gas turbine model combustor. Two mixture conditions, fuel molar ratio is  $X_{\text{CH}_4} : X_{\text{H}_2} = 1 : 1$  and  $4 : 1$  are simulated by using a reduced chemistry with 25 species and 111 reactions. The visualizations revealed that the flame shapes and the behaviors of H<sub>2</sub> are qualitatively different between the cases with different H<sub>2</sub>-enrichment ratios. For higher H<sub>2</sub>-enrichment ratio case, fuel species are almost consumed in the upstream, whereas the reaction zones locate in further downstream for lower H<sub>2</sub>-ratio case. To figure out the behaviors of H<sub>2</sub> in the flames, the conditionally averaged mass fractions and reaction rates are evaluated by comparing with unstrained and strained laminar flames. For the higher H<sub>2</sub>-ratio case, the H<sub>2</sub> mass fraction profile is similar to the unstrained and strained laminar flames on average. However, for the lower H<sub>2</sub>-ratio case, it deviates from the laminar profiles substantially. In addition, all of the conditionally averaged fuel species reaction rates are decreased and deviate from the laminar reaction rate profiles. These results suggest that the reaction zone profiles of swirling flames can not be predicted properly only by considering the effects of tangential strain rate. Therefore, the effects of transports might be more important than the chemical reactions and should be considered to elucidate the flame structures in detail.

### INTRODUCTION

Using H<sub>2</sub> as a fuel for combustion devices is one of the promising methods to achieve both thermal efficiency and reduced emissions of environmental pollutants, because of its great energy density and zero emissions of CO<sub>2</sub> during its combustion processes. However, there are still difficulties due to the characteristics of H<sub>2</sub> combustion (France, 1980). As an alternative method, H<sub>2</sub>-enriched natural gas has brought our attention. Advantages of using CH<sub>4</sub>/H<sub>2</sub> multi component fuel in lean premixed combustion are improved thermal efficiency with reduced emissions of environmental pollutants (Coppens *et al.*, 2007), extended lean blowout limit (Schefer, 2003) and resistance to strain rate induced extinction (Shanbhogue *et al.*, 2016). Thus, using such a fuel is considered to contribute to resolve recent environmental issues, because it can achieve both higher ther-

mal efficiency and reduced emissions of pollutants.

Gas turbine engines are considered as one of the predominant devices where utilization of the CH<sub>4</sub>/H<sub>2</sub> multi component fuel is effective. In such devices, turbulent swirling flows are widely used for flame stabilization and enhancement of turbulent mixing. Furthermore, relatively stronger three-dimensionality of the flow affects the flame structures and dynamics substantially. Therefore, understanding the structures of H<sub>2</sub>-enriched CH<sub>4</sub>/air turbulent premixed swirling flames is important for development of H<sub>2</sub>-enriched gas turbine engines.

Wang *et al.* (2009) have investigated chemical characteristics of H<sub>2</sub> in one-dimensional CH<sub>4</sub>/H<sub>2</sub>/air laminar premixed flames with various H<sub>2</sub> enrichment ratios. Their results suggest that the chemical characteristics of H<sub>2</sub> shifts from an intermediate species to a reactant species when the volume ratio of H<sub>2</sub> in the premixed mixture is increased from 20% to 30%. Day *et al.* (2011) have conducted 2-dimensional simulations of lean H<sub>2</sub>-enriched CH<sub>4</sub>/air turbulent premixed flames, which are categorized into the laminar flamelet regime. Here, the focus was on investigating the effects of the H<sub>2</sub> ratios on the local flame structures and C<sub>1</sub> and C<sub>2</sub> reaction pathways. They also concluded that the flame inner structure and H<sub>2</sub> show different behaviors when the H<sub>2</sub>-enrichment ratio is higher than 25%. These results indicate reaction pathway alternation with the increase of the H<sub>2</sub>/CH<sub>4</sub> ratios in both laminar and relatively low level turbulent flames. However, the effects of H<sub>2</sub>-enrichment ratios on the H<sub>2</sub>-enriched CH<sub>4</sub>/air turbulent swirling flame structures are not clarified yet. Therefore, in this study, direct numerical simulations (DNS) of H<sub>2</sub>-enriched CH<sub>4</sub>/air turbulent swirling premixed flames in a cuboid combustor have been conducted by using a reduced chemistry to clarify the effects of H<sub>2</sub> enrichment on the flame characteristics in H<sub>2</sub>-enriched natural gas turbine combustors.

### DNS OF TURBULENT SWIRLING FLAMES

The DNS code, called TTX (Tokyo Tech Combustion Simulation), developed by our previous works (Tanahashi *et al.*, 2000; Tanaka *et al.*, 2011) solves fully compressible governing equations with temperature dependency of transport and thermal properties by using CHEMKIN-II packages (Kee *et al.*, 1986, 1989) with vector and parallel computation modification. The governing equations are for conservation of mass, momentum, energy and species. The

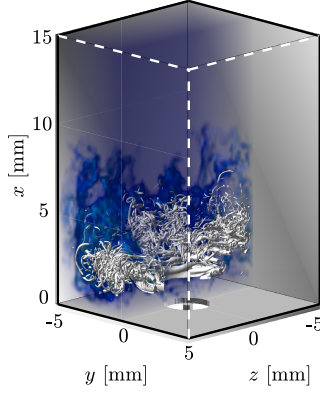


Figure 1. Schematics of the computational domain and coordinate system.

Table 1. Flame properties of one dimensional unstrained laminar conditions.

Case	$S_L$ [m/s]	$\delta_{th}$ [mm]	$\omega_{T,L}$ [W/m <sup>3</sup> ]
H <sub>2</sub> -50%	2.73	0.221	$1.63 \times 10^{10}$
H <sub>2</sub> -20%	1.97	0.249	$1.16 \times 10^{10}$

equations are discretized by using a fourth-order central finite difference scheme and advanced in time by a third-order Runge-Kutta scheme. The multi timescale (MTS) method (Gou *et al.*, 2010) is adopted for integration of chemical source terms and the correlated dynamic adaptive chemistry and transport (CO-DACT) method (Sun *et al.*, 2015; Sun & Ju, 2017) does for computing the transport and thermal properties of species. Navier-Stokes characteristic boundary condition (NSCBC) (Poinsot & Lele, 1992; Baum *et al.*, 1994) is imposed on the combustor walls, inflow and outflow boundaries. The effects of pressure gradient and the Soret diffusion are not considered in the calculation of the diffusion velocity. The Dufour effect is also neglected in the energy conservation equation. The detailed UCSD mechanism (Petrova & Williams, 2006) consisting of 57 species and 268 elemental reactions without nitrogen chemistry is reduced to 25 species and 111 reactions by the path flux analysis (PFA) method (Sun *et al.*, 2010).

Figure 1 shows schematics of the computational domain. The dimensions of combustor is  $L_x \times L_y \times L_z = 15 \text{ mm} \times 10 \text{ mm} \times 10 \text{ mm}$  and the number of uniform grid,  $N_x \times N_y \times N_z = 1152 \times 768 \times 768$ . The inlet boundary geometry is a concentric annulus of which inner and outer diameters are 0.6 mm and 2.5 mm, specified in the same manner as previous studies (Tanaka *et al.*, 2011; Aoki *et al.*, 2015; Minamoto *et al.*, 2015; Aoki *et al.*, 2017). The combustor wall is no-slip, inert and isothermal at 700 K. The stoichiometric mixture is preheated to 700 K at 0.1 MPa. Two mixture conditions with fuel species molar ratio;  $X_{CH_4} : X_{H_2}$  is 1 : 1 (H<sub>2</sub>-50%) and 4 : 1 (H<sub>2</sub>-20%) are simulated. These mixture conditions are determined to investigate the changes of the flame structures between different  $X_{CH_4} : X_{H_2}$  ratios. The flame properties, laminar flame speed  $S_L$ , flame thermal thickness  $\delta_{th} = (T_b - T_u)/|\nabla T|_{max}$  and the maximum heat release rate  $\omega_{T,L}$  for two mixture conditions are summarized in Table. 1.

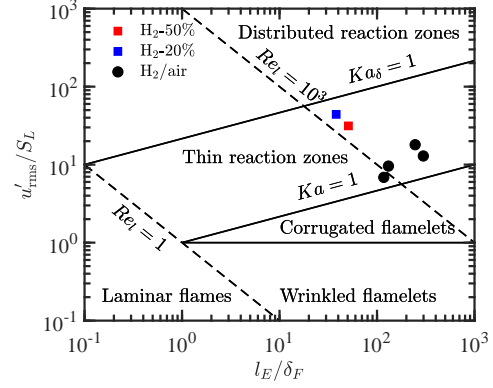


Figure 2. Turbulent combustion conditions of the present DNS (red and blue squares). The previously reported H<sub>2</sub>-air cases (Tanaka *et al.*, 2011; Aoki *et al.*, 2015; Minamoto *et al.*, 2015; Aoki *et al.*, 2017) are denoted by black circles.

Table 2. Parameters of the present DNS.  $u'_{rms}$  and  $l_E$  denote turbulence intensity, integral length scale.  $\delta_F$  denotes the Zel'dovich thickness ( $v_u/S_L$ ).  $Re_{l_E}$ ,  $Ka$  and  $Da$  is Reynolds number, Karlovitz number and Damköhler number based on  $l_E$ .

Case	$u'_{rms}/S_L$	$l_E/\delta_F$	$Re_{l_E}$	$Ka$	$Da$
H <sub>2</sub> -50%	31.4	50.9	1598	24.6	1.62
H <sub>2</sub> -20%	44.1	38.1	1680	47.4	0.86

The swirl number is 1.2 and the bulk mean axial velocity at the inlet,  $u_x^b$  is set to be 190 m/s to provide almost equivalent calorific input ( $\approx 1.16 \text{ kW}$ ) to the stoichiometric H<sub>2</sub>/air flames in the previous studies (Tanaka *et al.*, 2011; Aoki *et al.*, 2015). The inflow velocity perturbations,  $u'$  following the same manners to Wang *et al.* (Wang *et al.*, 2007) are added to the mean velocity profiles. The perturbations consist of simple white noise in which each frequency has a randomly-given lifetime for its phase. The maximum velocity perturbation intensity  $u'_{max}$  is  $0.15u_x^b = 28.5 \text{ m/s}$  and corresponding root mean square velocity fluctuation  $u'_{rms}$  at the inflow boundary is 10.5 m/s (about 5.5% of  $u_x^b$ ).

Figure 2 shows turbulent combustion conditions of the present study with previously reported H<sub>2</sub>/air cases (Tanaka *et al.*, 2011; Aoki *et al.*, 2015, 2017) on the combustion regime diagram (Peters, 2000). Several important non-dimensional parameters are listed in Table 2. Here,  $u'_{rms} = (2/3\bar{k})^{1/2}$  and  $l_E = (u'_{rms})^3/\bar{\epsilon}$ .  $\bar{k}$  is the turbulence kinetic energy and  $\bar{\epsilon}$  is the turbulent kinetic energy dissipation rate.  $\delta_F = v_u/S_L$  is the Zel'dovich thickness. The diagram is constructed base on volume averaged statistics in the region  $0.1 \leq \bar{c}_Y \leq 0.4$  by using 150 samples within the sampling period of  $300\mu\text{s}$ . Here,  $\bar{c}_Y$  is a Favre averaged reaction progress variable,  $c_Y \equiv (Y_s - Y_s^u)/(Y_s^b - Y_s^u)$ .  $Y_s \equiv Y_{H_2} + Y_{H_2O} + Y_{CO} + Y_{CO_2}$ , suggested in Ihme & Pitsch (2008a,b). The superscripts  $u$  and  $b$  denote the value of the unburnt and burnt gas sides in the corresponding laminar flame. As Fig. 2 shows, the turbulent flames are categorized in to the thin reaction zones regime. The Karlovitz numbers of present study are higher than those of H<sub>2</sub>/air cases, due to lower laminar burning velocities than H<sub>2</sub>/air flames.

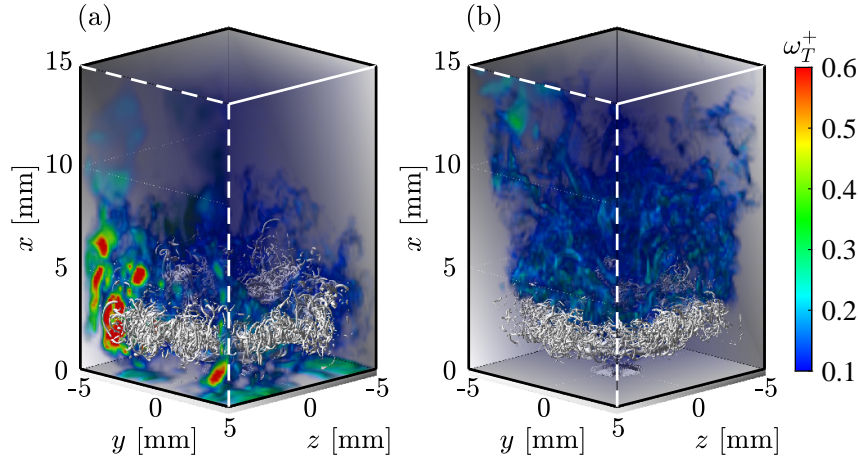


Figure 3. Instantaneous fields of normalized heat release rate  $\omega_T^+$  (volume rendered) and iso-surface of the second invariant of velocity gradient tensor  $Q^* = 0.01 Q_{\max}$  (white) for H<sub>2</sub>-50% (a) and H<sub>2</sub>-20% (b).

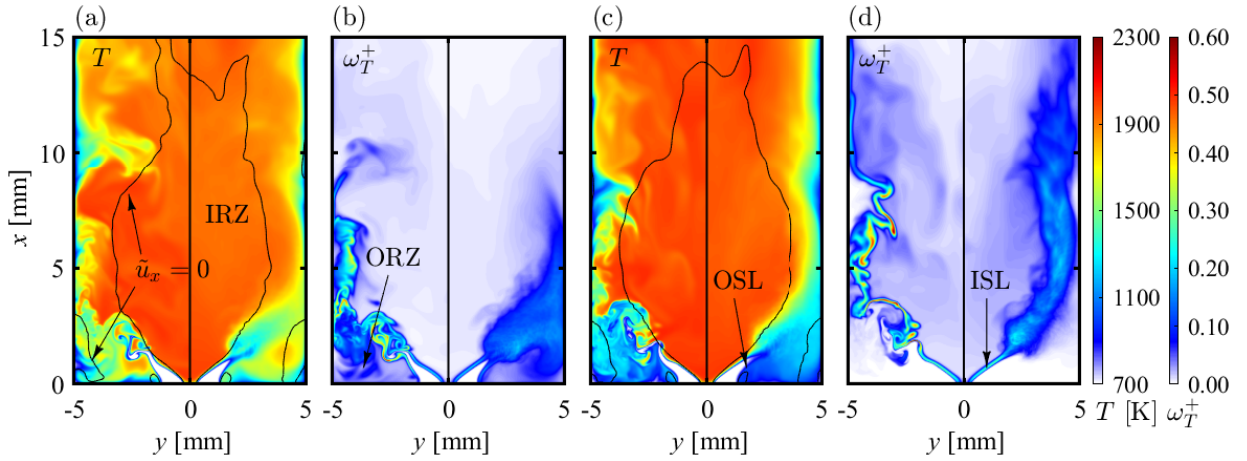


Figure 4. Instantaneous (left-half) and time-averaged (right-half) distributions of temperature  $T$ , contour lines of  $\tilde{u}_x = 0$  and normalized heat release rate  $\omega_T^+$  at the mid plane of the combustor for H<sub>2</sub>-50% (a, b) and H<sub>2</sub>-20% (c, d).

## H<sub>2</sub>-ENRICHMENT EFFECTS

To figure out the effects of H<sub>2</sub>-enrichment on the global flame features, instantaneous fields of heat release rate and the second invariant of velocity gradient tensor are shown in Fig. 3. The heat release rate is normalized as  $\omega_T^+ = \omega_T / \omega_{T,L}$ , where  $\omega_{T,L}$  is the maximum heat release rate of the corresponding laminar flame. The second invariant of velocity gradient tensor  $Q$  is computed as  $Q = 1/2(-S_{ij}S_{ij} + W_{ij}W_{ij})$ . Here,  $W_{ij}$  and  $S_{ij}$  is the symmetric and antisymmetric part of the velocity gradient tensor respectively. The threshold of  $Q^*$  field is 1% of its maximum. For both cases, larger-scale and an aggregation of fine-scale vortical structures are observed near the relatively upstream, due to strong shear layer and rapid development of turbulence. However, the shapes of  $\omega_T^+$  fields seem to be different between the different mixture conditions.

Figure 4 shows temperature and normalized heat release rate at the mid plane ( $z = 0$ ) of the combustor. The left-half of is for instantaneous and the right-half is for time-averaged distribution respectively. The contour lines are a Favre averaged axial velocity component  $\tilde{u}_x = 0$ . The inner recirculation zones (IRZ) where heat and combustion products are recirculated by the swirling flows are formed in the central part of the plane. At the corners of the plane, the outer recirculation zones (ORZ) are observed which re-

sulted from the existence of combustor walls. In this study, we refer the shear layer formed between the annular jets and IRZ or ORZ as the inner or outer shear layer (ISL or OSL) respectively.

For H<sub>2</sub>-50%,  $\omega_T^+$  is relatively high in the upstream region of the combustor and near to the combustor walls. On the other hand, for H<sub>2</sub>-20%, the high  $\omega_T^+$  region exists both in the upstream and downstream regions, whereas the  $\omega_T^+$  near the combustor walls is lower than 0.1. Focusing on the near field of annular jets, the magnitudes of  $\omega_T^+$  in the ISL and OSL are relatively similar for H<sub>2</sub>-50%. For H<sub>2</sub>-20%, however, the  $\omega_T^+$  is higher in the ISL rather than OSL. Furthermore, the temperature in the region spans from the OSL to the combustor walls are lower than H<sub>2</sub>-50% case. These different flame shapes between the cases are qualitatively similar to experimental observations of CH<sub>4</sub>/H<sub>2</sub> swirling flames with lower H<sub>2</sub>-enrichment ratios in literature (Cheng *et al.*, 2009; Shanbhogue *et al.*, 2016; Taamallah *et al.*, 2016).

To specify the distributions of the fuels in the combustor, the normalized species mass fractions,  $Y_i^*$  are shown in Fig. 5. The superscript “\*” denotes normalization by the value at the inflow boundary  $Y_i^u$ , hence,  $Y_i^* \equiv Y_i / Y_i^u$ . For H<sub>2</sub>-50%, the fuels are almost consumed in the upstream of the combustor (Figs. 5a and b). However, for H<sub>2</sub>-20%, the

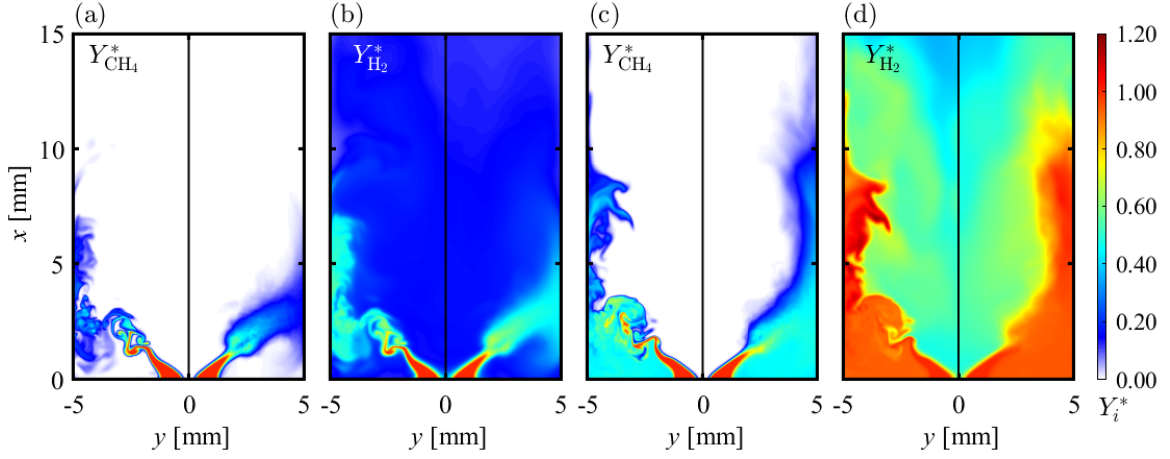


Figure 5. Instantaneous (left-half) and time-averaged (right-half) normalized species mass fractions,  $Y_i^*$  at the mid plane of the combustor for H<sub>2</sub>-50% (a, b) and H<sub>2</sub>-20% (c, d).

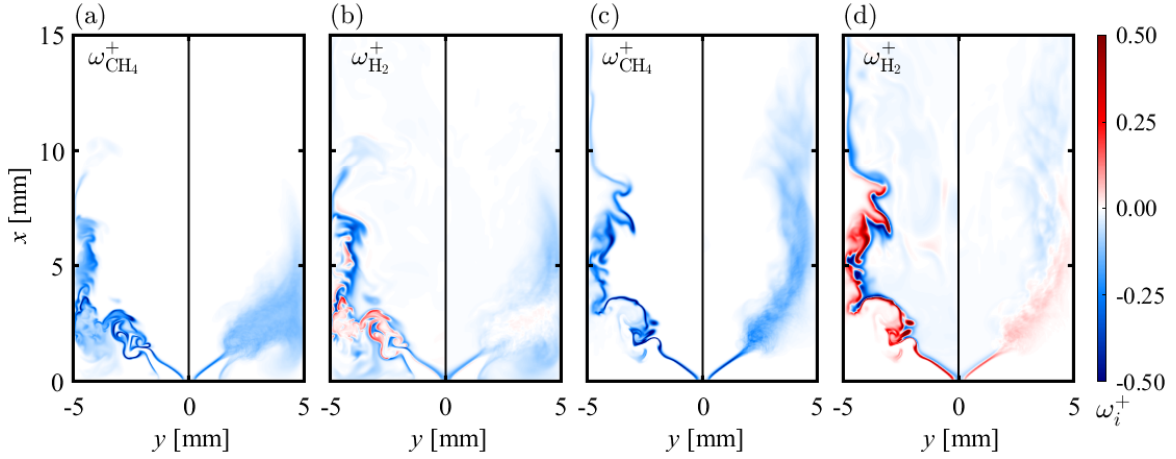


Figure 6. Instantaneous (left-half) and time-averaged (right-half) distributions of normalized fuel species reaction rates  $\omega_i^+$  at the mid plane of the combustor for the case of H<sub>2</sub>-50% (a, b) and H<sub>2</sub>-20% (c, d).

fuels remain in the region spans from the near field of OS� to relatively downstream of the combustor (Figs. 5c and d). Especially,  $Y_{H_2}^*$  is as high as or higher than  $Y_{CH_4}^*$  in the downstream. This implies that consumption of H<sub>2</sub> is suppressed and/or there is active production of H<sub>2</sub> for H<sub>2</sub>-20% case. These results suggest that H<sub>2</sub> shows different chemical behaviors with the increase of H<sub>2</sub>-ratios in the mixtures under relatively intense turbulence.

To clarify the chemical behaviors of the fuel species in detail, reaction rates of the fuels,  $\omega_{CH_4}^+$  and  $\omega_{H_2}^+$  are shown in Fig. 6. Here, the superscript “+” denotes normalization by  $\omega_{i,L}$ , which is the maximum of  $|\omega_i|$  in the corresponding laminar condition. Thus,  $\omega_i^+ \equiv \omega_i/\omega_{i,L}$ . Production and consumption reaction rates are colored by red and blue, respectively. Overall, the magnitudes of the fuel species reaction rates,  $|\omega_i^+|$  are decreased compared to the  $\omega_{i,L}$  in the present study, which is similar to previous studies (Tanaka *et al.*, 2011; Aoki *et al.*, 2015; Minamoto *et al.*, 2015; Aoki *et al.*, 2017). For both cases, only consumption of CH<sub>4</sub> can be observed in the combustor. However, for H<sub>2</sub>-20% case, the magnitudes of  $\omega_{CH_4}^+$  in the ORZ are noticeably reduced. As for  $\omega_{H_2}^+$ , both consumption and production reactions are observed. However, the tendencies are distinctively different between the cases. For H<sub>2</sub>-50%, consumption of H<sub>2</sub> is dominant in the upstream region and production of H<sub>2</sub> is

observed in the unburnt side of the reaction zones with relatively low magnitude. On the other hand, for H<sub>2</sub>-20%, consumption reaction occurs at the trailing edge of the flame, while production does in the unburnt side with relatively high magnitude. However, the magnitudes of  $\omega_{H_2}^+$  are very small in the ORZ. Therefore, the  $Y_i^*$  remaining relatively high in the region spans from the near field of OS� to the down stream region in Fig. 5d are mainly due to the slow chemistry in the ORZ.

Overall, the reaction rate contours suggest that both temperature and fuel species mass fraction fields consistently show different reaction zone locations between H<sub>2</sub>-50% and H<sub>2</sub>-20% cases under similar turbulent intensity. This indicates that even in strong turbulence, the chemical characteristics of H<sub>2</sub> are varied from an intermediate species to a reactant species with the increase of H<sub>2</sub> ratios.

## EVALUATIONS OF THE FLAME STRUCTURES IN PHASE SPACE

To evaluate the observed chemical characteristics, the conditional averages of  $Y_i^*$  conditioned based upon  $c_Y$ ,  $\langle Y_i^* | c_Y \rangle$  are examined. The unstrained and strained laminar flame profiles are superimposed to figure out the effects of tangential strain rate on the reaction zone profiles. The

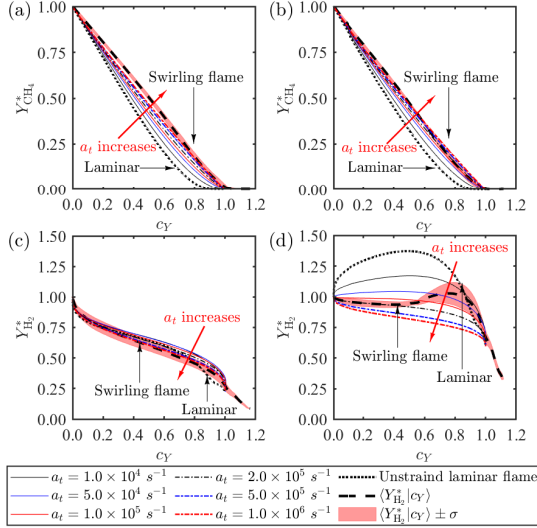


Figure 7. Conditional averages of the fuel species mass fractions,  $Y_i^*$  (dashed line) with respect to  $c_Y$  and standard deviation  $\pm\sigma$  about the mean (red surface) for H<sub>2</sub>-50% (a, c) and H<sub>2</sub>-20% (b, d). The arrow indicates increase of the tangential strain rate  $a_t$ .

superscript “\*” denotes the normalization by the value at the inflow boundary,  $Y_i^u$ . Here,  $c_Y$  can be larger than unity probably due to molecular transport to the burnt gas sides in the turbulent flames. In the process of conditional averaging, the samples obtained within approximately  $\delta_{th}$  from the wall are excluded to prevent the thermal boundary layers affecting the statistics. The thermochemical conditions of the strained laminar flames are set to be fresh reactants at fuel side ( $Y_i^u$  and  $T_u$ ) and burnt gases at oxidizer side ( $Y_i^b$  and  $T_b$ ), which are the identical values to the corresponding unstrained laminar flames. The tangential strain rate,  $a_t$  of the strained laminar flame is defined to be the first peak of velocity gradient,  $-du/dx$  in the reactant side. The values of  $a_t$  range from 2% to 200% of the mean strain rate in the unburnt gas sides of the DNS results, which is estimated to  $u'_{rms}/\lambda \approx 5.0 \times 10^5 \text{ s}^{-1}$ . Here,  $u'_{rms}$  is the velocity fluctuation and  $\lambda$  is the Taylor microscale.

As Fig. 7 shows, no significant difference is observed for  $Y_{CH_4}^*$  between the different mixture conditions. All of the  $Y_{CH_4}^*$  decrease monotonically with the increase of  $c_Y$  and the values decrease to nearly zero in the burnt gas sides. With the increase of  $a_t$ , the strained laminar profiles increase gradually for both cases, indicating decreased consumption of CH<sub>4</sub> with the increase of  $a_t$ . Furthermore, the  $\langle Y_{CH_4}^* | c_Y \rangle$  for both cases are similar to the strained laminar flames in which  $a_t \geq 5.0 \times 10^5 \text{ s}^{-1}$ , on average. Thus, the deviation from the corresponding unstrained laminar solution may suggest the decreased consumption of CH<sub>4</sub> and increased influences of molecular transport resulted from strong turbulent motions as shown in Fig. 6.

However, as for  $Y_{H_2}^*$ , substantial differences are observed between the cases with different fuel compositions in Figs. 7c and d. For H<sub>2</sub>-50% case,  $\langle Y_{H_2}^* | c_Y \rangle$  shows relatively similar behaviors to the laminar profiles on average in the entire  $c_Y$  region. The strained laminar flame profile decreases slightly with the increase of  $a_t$ . However, for H<sub>2</sub>-20% case,  $\langle Y_{H_2}^* | c_Y \rangle$  deviates from the corresponding unstrained and strained laminar values in the unburnt gas sides,  $c_Y \lesssim 0.6$ . Such  $Y_{H_2}^*$  values as high as its inflow

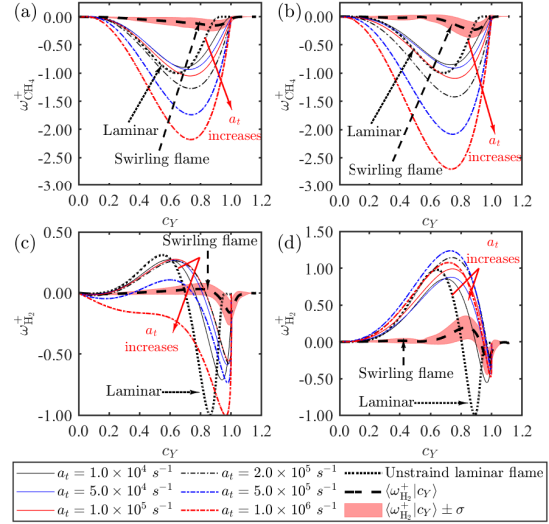


Figure 8. Conditional averages of the fuel species reaction rates,  $\omega_i^+$  (dashed line) with respect to  $c_Y$  and standard deviation  $\pm\sigma$  about the mean (red surface) for H<sub>2</sub>-50% (a, c) and H<sub>2</sub>-20% (b, d). The arrow indicates increase of the tangential strain rate  $a_t$ .

value correspond to the observations in the near wall region of Fig. 5d. Furthermore, the values of  $Y_{H_2}^*$  for the strained flames decrease gradually with the increase of  $a_t$ , suggesting higher sensitivity of  $Y_{H_2}^*$  to  $a_t$  than H<sub>2</sub>-50% composition.

To figure out the responses of  $Y_i^*$  to the  $a_t$  in detail, the fuel species reaction rate profiles in  $c_Y$  space are shown in Fig. 8. The superscript “+” denotes normalization by  $\omega_{i,L}$ , the maximum of  $|\omega_i|$  in the corresponding unstrained laminar flames,  $\omega_i^+ = \omega_i/\omega_{i,L}$ . For both of the mixture conditions, the responses of  $\omega_{CH_4}^+$  to the  $a_t$  are relatively similar. With the increase of  $a_t$ ,  $|\omega_{CH_4}^+|$  increase in the entire  $c_Y$  region, which suggests the increased influences of molecular transport. On the other hand, the responses of  $\omega_{H_2}^+$  to the  $a_t$  are more sensitive for H<sub>2</sub>-50% composition, which is an opposite tendency to the observed one in the responses of  $Y_{H_2}^*$  to the  $a_t$  in Fig. 7. However, all of the conditionally averaged reaction rates in the swirling flames deviate from the laminar profiles in the entire  $c_Y$  region. These reaction rate profiles suggest that the reaction zone profiles of the swirling flames can not be predicted properly only by considering the effects of tangential strain rate. This indicates that effects of turbulent strain rate should be taken into account to figure out the deviations in detail. Furthermore, the effects of molecular transport seem to be more influential than the chemical reactions and need to be investigated.

## CONCLUSIONS

To clarify the effects of H<sub>2</sub>-enrichment on the flame structures in a CH<sub>4</sub>/H<sub>2</sub> multi component fuel gas turbine combustor, direct numerical simulations of stoichiometric H<sub>2</sub>-enriched CH<sub>4</sub>/air turbulent swirling premixed flames in a cuboid combustor have been performed. Two mixture conditions, of which volume ratio of CH<sub>4</sub>:H<sub>2</sub> = 1:1 (H<sub>2</sub>-50%) and 4:1 (H<sub>2</sub>-20%) are simulated by using a reduced chemistry (25 species and 111 elemental reactions).

Overall, the results suggest that H<sub>2</sub> shows different chemical characteristics with the increase of H<sub>2</sub>-enrichment ratios. This indicates that reaction pathways alternation

of H<sub>2</sub>, the role of H<sub>2</sub> shifts from an intermediate species to a reactant species, reported in Wang *et al.* (2009) and Day *et al.* (2011) are also observed even in strong turbulence. The differences induced by different H<sub>2</sub> ratios in the mixture conditions are pronounced in the ORZ and downstream. For H<sub>2</sub>-50% case, the reaction zones are observed in the upstream due to rapid consumption of the fuel species in the near field of the OSL and ORZ. For H<sub>2</sub>-20% case, however, the reaction zones locate in further downstream due to the slow chemistry in the OSL and ORZ.

The conditionally averaged mass fraction profiles of CH<sub>4</sub> and H<sub>2</sub> for H<sub>2</sub>-50% case are similar on average to the unstrained and strained laminar flames, whereas H<sub>2</sub> mass fraction profile for H<sub>2</sub>-20% case deviates from the laminar profiles. Furthermore, all of the averaged fuel species reaction rates in the swirling flames deviate from the laminar reaction rate profiles. The results suggest that the reaction zone profiles of the turbulent swirling flames can not be predicted properly only by considering the effects of tangential strain rate. It also indicates that other types of transports, such as turbulent and molecular diffusion are more important than the chemical reactions in the present DNS and the effects of turbulent strain rate should be considered.

## REFERENCES

- Aoki, K., Shimura, M., Naka, Y. & Tanahashi, M. 2017 Disturbance energy budget of turbulent swirling premixed flame in a cuboid combustor. *Proceedings of the Combustion Institute* **36** (3), 3809–3816.
- Aoki, K., Shimura, M., Ogawa, S., Fukushima, N., Naka, Y., Nada, Y., Tanahashi, M. & Miyauchi, T. 2015 Short- and long-term dynamic modes of turbulent swirling premixed flame in a cuboid combustor. *Proceedings of the Combustion Institute* **35** (3), 3209–3217.
- Baum, M., Poinso, T. & Thévenin, D. 1994 Accurate boundary conditions for multicomponent reactive flows. *Journal of Computational Physics* **116** (2), 247–261.
- Cheng, R. K., Littlejohn, D., Strakey, P. A. & Sidwell, T. 2009 Laboratory investigations of a low-swirl injector with H<sub>2</sub> and CH<sub>4</sub> at gas turbine conditions. *Proceedings of the Combustion Institute* **32 II** (2), 3001–3009.
- Coppens, F. H. V., De Ruyck, J. & Konnov, A. A. 2007 The effects of composition on burning velocity and nitric oxide formation in laminar premixed flames of CH<sub>4</sub> + H<sub>2</sub> + O<sub>2</sub> + N<sub>2</sub>. *Combustion and Flame* **149** (4), 409–417.
- Day, M. S., Gao, X. & Bell, J. B. 2011 Properties of lean turbulent methane-air flames with significant hydrogen addition. *Proceedings of the Combustion Institute* **33** (1), 1601–1608.
- France, D. H. 1980 Combustion characteristics of hydrogen. *International Journal of Hydrogen Energy* **5** (4), 369–374.
- Gou, X., Sun, W., Chen, Z. & Ju, Y. 2010 A dynamic multi-timescale method for combustion modeling with detailed and reduced chemical kinetic mechanisms. *Combustion and Flame* **157** (6), 1111–1121.
- Ihme, M. & Pitsch, H. 2008a Prediction of extinction and reignition in nonpremixed turbulent flames using a flamelet/progress variable model. 1. A priori study and presumed PDF closure. *Combustion and Flame* **155** (1-2), 70–89.
- Ihme, M. & Pitsch, H. 2008b Prediction of extinction and reignition in nonpremixed turbulent flames using a flamelet/progress variable model. 2. Application in LES of Sandia flames D and E. *Combustion and Flame* **155** (1-2), 90–107.
- Kee, R. J., Dixon-Lewis, G., Warnatz, J., Coltrin, M. E. & Miller, J. A. 1986 *A Fortran computer code package for the evaluation of gas-phase multicomponent transport properties*. Report No. SAND86-8246, Sandia National Laboratories.
- Kee, R. J., Rupley, F. M. & Miller, J. A. 1989 *Chemkin-II: A Fortran chemical kinetics package for the analysis of gas phase chemical kinetics*. Report No. SAND89-8009B, Sandia National Laboratories.
- Minamoto, Y., Aoki, K., Tanahashi, M. & Swaminathan, N. 2015 DNS of swirling hydrogen-air premixed flames. *International Journal of Hydrogen Energy* **40** (39), 13604–13620.
- Peters, N. 2000 *Turbulent combustion*. Cambridge, U.K.: Cambridge University Press.
- Petrova, M. V. & Williams, F. A. 2006 A small detailed chemical-kinetic mechanism for hydrocarbon combustion. *Combustion and Flame* **144** (3), 526–544.
- Poinso, T. J. & Lele, S. K. 1992 Boundary conditions for direct simulations of compressible viscous flows. *Journal of Computational Physics* **101** (1), 104–129.
- Schefer, R. W. 2003 Hydrogen enrichment for improved lean flame stability. *International Journal of Hydrogen Energy* **28** (10), 1131–1141.
- Shanbhogue, S. J., Sanusi, Y. S., Taamallah, S., Habib, M. A., Mokheimer, E. M. A. & Ghoniem, A. F. 2016 Flame macrostructures, combustion instability and extinction strain scaling in swirl-stabilized premixed CH<sub>4</sub>/H<sub>2</sub> combustion. *Combustion and Flame* **163**, 494–507.
- Sun, W., Chen, Z., Gou, X. & Ju, Y. 2010 A path flux analysis method for the reduction of detailed chemical kinetic mechanisms. *Combustion and Flame* **157** (7), 1298–1307.
- Sun, W., Gou, X., El-Asrag, H.A., Chen, Z. & Ju, Y. 2015 Multi-timescale and correlated dynamic adaptive chemistry modeling of ignition and flame propagation using a real jet fuel surrogate model. *Combustion and Flame* **162** (4), 1530–1539.
- Sun, W. & Ju, Y. 2017 A multi-timescale and correlated dynamic adaptive chemistry and transport (CO-DACT) method for computationally efficient modeling of jet fuel combustion with detailed chemistry and transport. *Combustion and Flame* **184**, 297–311.
- Taamallah, S., Shanbhogue, S. J. & Ghoniem, A. F. 2016 Turbulent flame stabilization modes in premixed swirl combustion: Physical mechanism and Karlovitz number-based criterion. *Combustion and Flame* **166**, 19–33.
- Tanahashi, M., Fujimura, M. & Miyauchi, T. 2000 Coherent fine scale eddies in turbulent premixed flames. *Proceedings of the Combustion Institute* **28** (2), 529–535.
- Tanaka, S., Shimura, M., Fukushima, N., Tanahashi, M. & Miyauchi, T. 2011 DNS of turbulent swirling premixed flame in a micro gas turbine combustor. *Proceedings of the Combustion Institute* **33** (2), 3293–3300.
- Wang, J., Huang, Z., Tang, C., Miao, H. & Wang, X. 2009 Numerical study of the effect of hydrogen addition on methane-air mixtures combustion. *International Journal of Hydrogen Energy* **34** (2), 1084–1096.
- Wang, Y., Tanahashi, M. & Miyauchi, T. 2007 Coherent fine scale eddies in turbulence transition of spatially-developing mixing layer. *International Journal of Heat and Fluid Flow* **28**, 1280–1290.